Direct imaging shows that insulin granule exocytosis occurs by complete vesicle fusion

Li Ma*†, Vytautas P. Bindokas†‡, Andrey Kuznetsov*, Christopher Rhodes§, Lori Hays§, J. Michael Edwardson¶, Kazuya Ueda‖, Donald F. Steiner‖, and Louis H. Philipson*,**

Departments of *Medicine, ‡Neurobiology, Pharmacology and Physiology, and ‖Biochemistry and Molecular Biology and ‖Howard Hughes Medical Institute, University of Chicago, Chicago, IL 60637; §Pacific Northwest Research Institute, Seattle, WA 91822; and ¶Department of Pharmacology, University of Cambridge, Tennis Court Road, Cambridge CB2 1PD, United Kingdom

Contributed by Donald F. Steiner, May 6, 2004

Confocal imaging of GFP-tagged secretory granules combined with the use of impermeant extracellular dyes permits direct observation of insulin packaged in secretory granules, trafficking of these granules to the plasma membrane, exocytotic fusion of granules with the plasma membrane, and eventually the retrieval of membranes by endocytosis. Most such studies have been done in tumor cell lines, using either confocal methods or total internal reflectance microscopy. Here we compared these methods by using GFP–syncollin or PC3–GFP plus rhodamine dextrans to study insulin granule dynamics in insulinoma cells, normal mouse islets, and primary pancreatic beta cells. We found that most apparently docked granules did not fuse with the plasma membrane after stimulation. Granules that did fuse typically fused completely, but a few dextran-filled granules lingered at the membrane. Direct recycling of granules occurred only rarely. Similar results were obtained with both confocal and total internal reflection microscopy, although each technique had advantages for particular aspects of the granule life cycle. We conclude that insulin exocytosis involves a prolonged interaction of secretory granules with the plasma membrane, and that the majority of exocytotic events occur by full, not partial, fusion.

Secretory cells typically release hormones and neurotransmitters by regulated, Ca^{2+}-dependent exocytosis of vesicles or granules (1). Regulated exocytosis is a multistage process involving transport of granules to the plasma membrane, docking of the vesicles with the plasma membrane, and fusion causing release of the contents. Insulin is transported in pancreatic beta cells in large dense core vesicles (LDCV), termed secretory granules. A healthy beta cell maintains in excess of 10,000 granules, but not all granules are functionally equivalent (2, 3). Roughly 1,000 granules are morphologically docked to the plasma membranes, and perhaps 100 of these are in a readily releasable pool. Only a small proportion of total insulin is released even under maximal stimulatory conditions (4, 5). Mechanisms that control transfer of granules to the readily releasable pool as well as details of release activation remain unresolved. Numerous studies have demonstrated kiss-and-run secretory events in several types of cells, but is this type of release the predominant mechanism for LDCVs containing large crystals of insulin? Direct visualization of insulin granule exocytosis by methods in primary cells that minimize artifacts would greatly aid the understanding of the processes involved in their regulated fusion.

Regulated exocytosis in neuroendocrine cells is thought to be spatially and temporally coordinated with endocytic retrieval of secretion vesicle membranes (6). Recent investigations have used vesicle-associated fluorescent dyes and GFP-tagged LDCV-associated proteins or insulin itself, and imaging with conventional, total internal reflection fluorescence (TIRF), or confocal microscopy (7–10). Fusion events are inferred by the loss of fluorescence at the cell surface (fluorescent vesicle proteins, "recycled" membrane dyes, or acidophilic dyes) or by the increased fluorescence associated with neutralization of granule pH (11). These studies have generally concluded that LDCVs are recruited to the plasma membrane and may make multiple partial fusions before fully fusing and releasing the granule contents (flickering and/or kiss-and-run fusions) (6, 12, 14). Insulin is stored as a crystal, made up of hexamers that will need to diffuse out and dissociate into monomers. Momentary openings may not allow the crystal to dissolve and the large protein to diffuse away. LDCVs offer distinct advantages for study of regulated exocytosis for several reasons. The LDCVs have large diameters (≈300 nm for insulin granules, i.e., 10 times bigger than synaptic vesicles) that aid resolution of single vesicles and fusion events. Release of LDCVs is very tightly regulated, requiring high ambient calcium or specific stimuli for exocytosis. Relatively few LDCVs may be docked and released at one time, aiding tracking of single events. Current optical and electrophysiological approaches to study these processes in parallel or simultaneously have not yet led to a full understanding of the underlying mechanisms (1, 7–9).

We investigated the exocytosis of individual insulin granules by using the high spatial resolution and optical sectioning capability of standard single photon laser scanning confocal microscopy. We followed insulin granules in pancreatic beta cells labeled with either GFP fused with the LDCV-associated protein syncollin (syncollin–GFP) (15) or granule-targeted prohormone convertase protein-3 (PC3–GFP) (16). We found both granule-associated proteins syncollin and PC3 only labeled newly synthesized LDCV granules. When combined with bathing the living cell in a fluorescent fluid-phase tracer dye (primarily 3-kDa dextran-tetramethylrhodamine; dextran–TMR) high-speed confocal imaging allowed simultaneous determination of the opening of the fusion pore, and the kinetics of granule fusion. We found that most fusing granules rapidly filled with extracellular dye and collapsed completely as the fusion event progressed. Only a few granules (<5%) opened without collapse of the granule membrane into the surface membrane, and these were immediately retrieved back into the cell during stimulation. These results were similar to those obtained with TIRF microscopy using fluorescently tagged syncollin–GFP to follow the fate of insulin granule contents during exocytosis after a secretory stimulus.

Materials and Methods

Cell Culture. Islets and dispersed islet cells were isolated from pancreata of 8- to 10-week-old C57BL/6J mice (The Jackson Laboratory) using collagenase digestion followed by discontinuous Ficoll gradient centrifugation. Islet cells were dissociated by using 0.25 mg/ml trypsin. Cells or islets were cultured on glass coverslips and incubated in RPMI medium 1640 containing 11.5

Abbreviations: LDCV, large dense core vesicles; TIRF, total internal reflection fluorescence; PC3, prohormone convertase 3.

†L.M. and V.P.B. contributed equally to this work.

**To whom correspondence should be addressed. E-mail: l-philipson@uchicago.edu.

www.pnas.org/cgi/doi/10.1073/pnas.0403201101

mM glucose, 10% FBS, 100 units/ml penicillin, and 100 μg/ml streptomycin at 37°C for 1–2 days before transduction (17). MIN6 cells (18) were grown in DMEM (Life Technologies) containing 25 mM glucose, 10% FBS, 100 units/ml penicillin, and 100 μg/ml streptomycin.

Recombinant Replication-Deficient Adenoviruses Expressing Syncollin–GFP. Syncollin–pEGFP-N1 was transformed into DM1 cells and subsequently subcloned into pShuttle–CMV adenoviral vector (Quantum Biotechnologies, Montreal) (15). Recombinant adenovirus was generated by using the bacterial recombination method as described (19). The adenoviral genomic and shuttle vectors containing the syncollin–GFP insert were recombined in transfected *Escherichia coli* BJ5183 cells, recombinant vector was purified from a single plaque colony and transfected into HEK-293 cells that subsequently generated a recombinant adenovirus. Recombinant adenovirus was amplified and purified from HEK-293 cell lysates and used in gene transfer experiments into islets and beta cell lines (20). Viruses used for islet and MIN6 cells infection were plaque-purified, collected by CsCl isopycnic centrifugation, dialyzed with Hepes-buffered saline (140 mM NaCl/2 mM $MgCl_2$/10 mM Hepes, pH 7.5) containing 10% glycerol, stored at −80°C in small aliquots, and titered by plaque assay.

The Construct of EGFP-Tagged PC3. A truncated rat PC3 cDNA (1–616) (16) was amplified by PCR with specific primers incorporating *Hin*dIII and *Bam*HI sites, and subcloned 5′ to the EGFP site in the pEGFP-N3 vector (Clontech). The construct was verified by sequencing.

Transduction. Culture medium was removed, cells were washed once, and then medium was replaced with medium containing 2% (vol/vol) heat-inactivated FBS and purified virus (200 plaque forming units per cell). Cells and islets were incubated at 37°C for 1 and 10 h, respectively. Cultures were washed and incubated in complete medium at 37°C. MIN6 cells were transfected with pPC3–GFP by using Effectene reagent (Qiagen, Valencia, CA). All experiments were performed 5–48 h after transfection.

Immunofluorescence. After adenovirus (AdV)–syncollin–GFP or pPC3–GFP transduction, cells were fixed with 4% paraformaldehyde in PBS, washed with PBS alone, and incubated overnight at 4°C in 2% BSA/PBS containing guinea pig anti-insulin antibody (1:1,000; Dako). The cells were incubated in 2% donkey serum/PBS for 30 min, and exposed to Cy3-conjugated donkey anti-guinea pig IgG (1:500; Jackson ImmunoResearch) for 60 min at room temperature (19). Insulin immunostaining and GFP expression were visualized by using laser scanning confocal microscopy.

Optical Imaging. Cells were imaged with an IX70 Olympus Fluoview 200 laser-scanning confocal microscope (Melville, NY) equipped with three lasers (488-nm Ar, 543- and 633-nm He–Ne), ×60 PlanApo (numerical aperture, 1.4 oil), and ×100 UplanApo (numerical aperture, 1.35 oil) objectives, and differential interference contrast optics. Detectors (12-bit) were set to accommodate the brightest image. Digital scan zoom (×4–5) was used to improve resolution. Green (GFP) and red (dextran–TMR) fluorescence emission channels were collected simultaneously by using dual-laser line excitation (488 nm and 543 nm). Images were corrected for channel cross-talk. Data were collected at 1.3–1.7 Hz because most vesicle fusion events appeared to last several seconds. Cells and islets were superfused with Krebs–Ringer buffer containing 119 mM NaCl, 4.7 mM KCl, 25 mM $NaHCO_3$, 2.5 mM $CaCl_2$, 1.2 mM $MgSO_4$, 1.2 mM KH_2PO_4, and 25 mM glucose (MIN6 cells) or 11 mM (beta cells or islets) (17). All imaging experiments were conducted at 35–37°C.

TIRF Microscopy. TIRF studies were conducted on an Olympus IX81 inverted microscope, using an argon laser (488 nm; up to 10 mW), a TIRF illuminator, a ×60 numerical aperture 1.45 objective, and occasionally the ×1.6 magnification changer. Illumination angle was set to produce the shallowest evanescent illumination (≈100 nm). Images were collected on a Retiga EXi chilled charged coupled device (QImaging, Burnaby, BC, Canada), 30- to 100-ms exposures/10–30 frames per second, under control of METAMORPH software (Universal Imaging, Downingtown, PA).

Image Analysis. Images were analyzed by using METAPORPH image processing software or NIH IMAGE J (Wayne Rasband, Research Services Branch, National Institute of Mental Health, Bethesda). Animations of 3D reconstructions were created with METAPORPH or VOXX (21). Colocalization of GFP and dextran–TMR omega figures was determined from image overlays. Image processing was used to determine the dynamics of dextran–TMR labeling. Differences in the fluorescence intensity between consecutive image pairs were used to create derivative images ($image_n - image_{n-1}$). Diameters of GFP granules and omegas were determined by morphometric analysis.

Results

We initially compared PC3–GFP and syncollin–GFP for cellular localization and for colocalization with insulin-containing LDCVs in MIN6 insulinoma cells, isolated islets, and dispersed beta cells. Previous work has demonstrated that syncollin–GFP can be correctly targeted to LDCVs in AtT-20 pituitary cells (15). GFP tagging significantly alters the properties of syncollin. In AtT-20 cells, syncollin itself significantly reduces regulated exocytosis of ACTH, whereas GFP-tagged syncollin does not (22). When insulin-secreting cells were transfected with adenovirus–syncollin–GFP (AdV–syncollin–GFP) or PC3–GFP, GFP fluorescence was associated with only new vesicles. We found that fusing GFP with a protein associated with the vesicle inner membrane (syncollin–GFP) or within the lumen (PC3–GFP) had no obvious effect on granule fusion, and syncollin–GFP did not inhibit insulin secretion (data not shown).

Syncollin–GFP expression in the MIN6 cells first became evident 5–6 h after infection with adenovirus. A weak cytoplasmic fluorescence sometimes appeared, perhaps corresponding to endoplasmic reticular pools; however, most of the GFP fluorescence remained associated with vesicular structures. The granule-like, fluorescent puncta later appeared near the nucleus, consistent with Golgi localization (Fig. 1). After ≈8 h, many fluorescent spots of a uniform size were distributed throughout the cells, and some appeared to associate with the plasma membrane (Fig. 1*A*, arrows). These patterns persisted beyond 12–24 h, and were observed for up to 48 h. Similar results were observed in pancreatic beta cells (Fig. 1*B*). PC3–GFP expression in MIN6 cells followed a similar pattern and time course to those observed with syncollin–GFP (Fig. 1*C*)

Targeting efficiency of syncollin–GFP to insulin-containing LDCVs was evaluated by immunostaining and quantitative colocalization imaging using confocal microscopy. Syncollin–GFP was present in insulin granules in primary pancreatic beta cells (Fig. 2 *A* and *B*) and in MIN6 cells (Fig. 2*C*). Fig. 2*A* shows an orthogonal projection through an optically sectioned beta cell. Syncollin–GFP and insulin displayed complete (yellow) or partial colocalization (green or red; Fig. 2 *B*, asterisk, and *C*, arrow). After 48-h infection, the average colocalization of syncollin–GFP and insulin was 76 ± 6% ($n = 4$ cells) in pancreatic beta cells and 80 ± 8% ($n = 5$ cells) in MIN6 cells. Movie 1, which is published as supporting information on the PNAS web

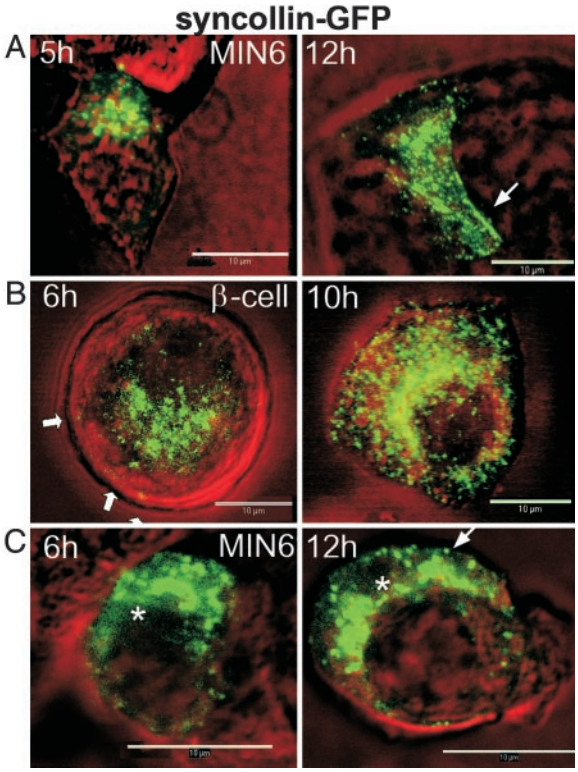

Fig. 1. Time course of syncollin–GFP expression in MIN6 (*A*) and mouse (*B*) beta cells and PC3–GFP in MIN6 cells (*C*). Images represent typical appearance of expression in cells at times indicated. Arrows indicate regions with peripheral punctate fluorescence. Asterisks indicate regions of diffuse fluorescence. (Scale bars = 10 μm.)

site, shows a computer-generated three-dimensional reconstruction of the colocalization of syncollin–GFP and insulin from multiple *z* axis optical sections of the cell shown in Fig. 2*C*. The pattern of colocalization of syncollin–GFP and insulin as well as granule distribution in MIN6 cells was similar to that in primary beta cells. Coregistration of insulin staining and syncollin–GFP

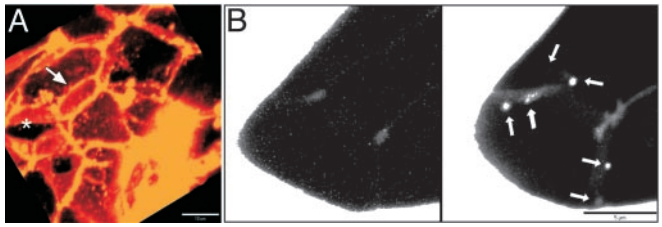

Fig. 3. Three-dimensional intercellular distribution of 3-kDa dextran–TMR in a mouse islet (XYZ). (*A*) Three-dimensional reconstruction of confocal images of dextran–TMR fluorescence obtained ≈5 min after application to live mouse islets. White arrows indicate bright ''creases'' at intersections between multiple beta cells. Asterisks indicate areas of uniform, less intense staining of narrow spaces between cells. Similar patters are obtained with FM-464 after staining (data not shown). (*B*) Maximum intensity projections of bright dextran–TMR-bathed unstimulated a mouse islet (*Left*) and same cells after depolarization with 40 mM KCl (*Right*). Omega-like figures (arrows) appear after depolarization (see Movie 2). Here, bright spots (arrows) indicate sites of rapidly changing dextran–TMR-filled profiles that mainly occur at cell edges. (Scale bars, 10 μm in *A* and 5 μm in *B*.)

is shown in two additional beta cells (Fig. 2*B*). The average diameter of syncollin–GFP granules was 318 ± 43 nm (n = 6,319 granules). The average number of LDCVs in MIN6 cells was 2,412 ± 563 granules per cell. This is in close agreement with measurements of the average diameter (311 ± 45 nm) and number (3,290 granules per MIN6 cell) of immunostained insulin granules and values reported in other studies (2–4).

For simultaneous observation of exocytosis and the membrane surface endocytosis we used 3-kDa dextran–TMR, a red fluorescent membrane-impermeable fluid-phase tracer. Application of dextran–TMR to the external surface of the cell allowed high-contrast visualization of the cell surface. The dye rapidly filled the intercellular spaces in monolayers of MIN6 cells and single intact islets of Langerhans (Fig. 3*A*). A similar staining pattern was obtained with sulforhodamine B (SRB), a smaller fluorescent molecule, but single-photon excitation of SRB produced rapid phototoxicity, thus precluding its use in our studies.

Exocytotic fusion of LDCVs would allow access of dextran–TMR to the intravesicular space through the fusion pore leading

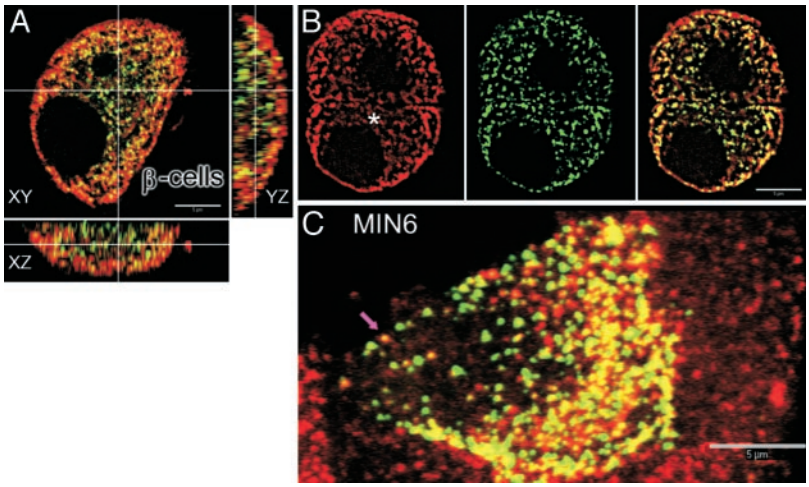

Fig. 2. Colocalization of syncollin–GFP and insulin in beta (*A* and *B*) and MIN6 (*C*) cells. Colocalization of fluorescence is greater near cell periphery than in the perinuclear region. (*A*) Orthogonal views (XY, XZ, YZ) through one beta cell demonstrating localization of syncollin–GFP (green) and insulin staining (Cy3, red); colocalization produces yellow color. (*B*) Single optical section showing insulin staining (*Left*, red) in cell interior (asterisk) and syncollin–GFP (*Center*, green). (*Right*) Overlay image. (*C*) Three-dimensional maximum intensity reconstruction of a MIN6 cell showing colocalization (arrow) of insulin (red) and syncollin–GFP (green). Animated reconstructions (see Movie 1) show cellular distribution of both probes as well as the degree of colocalization per vesicle. (Scale bars, 5 μm.)

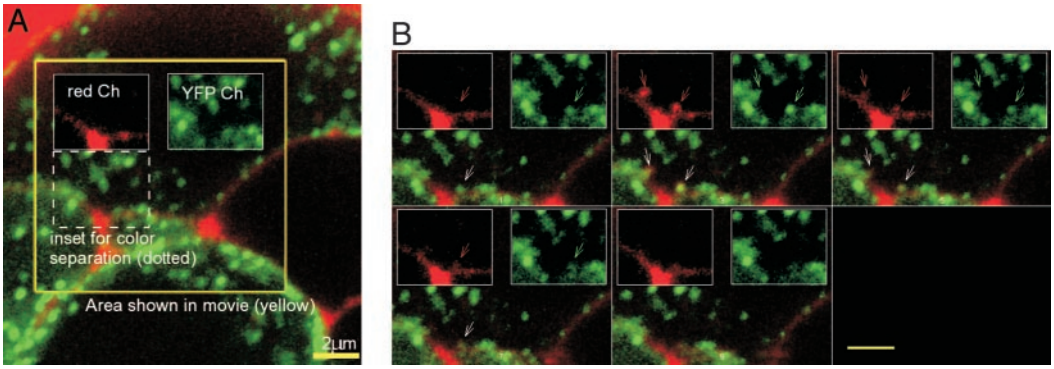

Fig. 4. Exocytosis of GFP–syncollin-labeled granules in MIN6 cells. See Movie 3 for full experiment (panels show 66.3–120.9 s, upper left to lower right, after 40 K^+ addition). Two fusions (arrows) occurring at the right edge of a MIN6 cell are indicated in frames with asterisks. Filling of the green (GFP) insulin granule with extracellular dextran–TMR results in a yellow structure. Note that some dextran filled structures slightly expand beyond the diameter of the associated GFP vesicles and that most dextran-filled granules fully disappear (see Movie 3, 147-s total duration, and see Movie 4). Image sample rate was 0.9 s per image. (Scale bar, 3 μm.)

to the appearance of a transient irregularity at the membrane surface. During observations totaling 1 h, unstimulated MIN6 cells ($n = 20$) and single intact islets ($n = 10$) did not exhibit transient omega-shaped regions, indicating a low level of constitutive exocytosis of LDCVs (Fig. 3*B Left*) and absence of light-induced events. However, 20–30 s after depolarization with 40 mM KCl, transient punctate, omega-like regions filled with dextran–TMR appeared (Fig. 3*B Right*). In cross-section, the membrane region stained with dextran–TMR was shaped like an inverted Greek omega and is similar to the ultrastructural morphology of membrane-fused LDCVs observed with transmission electron microscopy (23–25). The size (Fig. 3*B*, arrows; average diameter, 265 ± 30 nm; $n = 29$) and morphology of the omega-like figures were also consistent with LDCV exocytosis of insulin-containing granules visualized by TIRFM imaging of insulin–GFP (1). Most of the events were located on cell borders, although occasionally we observed staining within the cytoplasm (Fig. 3*B*, uppermost arrow; see Movie 2, which is published as supporting information on the PNAS web site). Similar results were also observed in MIN6 cells (data not show).

The average amount of time that an omega structure remained at the plasma membrane was 10.1 ± 1.8 s (mean ± SEM, $n = 74$), and ranged between 0.24 and 82 s, nearly always fully collapsing to a smooth surface. We seldom observed mobile LDCVs within the cytoplasm that contacted the plasma membrane transiently and filled with dextran–TMR (virtually no kiss-and-run). The median onset time of dextran–TMR-labeled events after depolarization was 50.3 s, similar to previous reports using other methods (9).

Vesicles expressing syncollin–GFP within the cytoplasm exhibited Brownian motion and directed, saltatory transport similar to the observations in unlabeled beta cells (26). However, granules adjacent to the inner surface of the plasma membrane were immobile, possibly indicative of docking. In unstimulated primary beta cells, the docked vesicles did not undergo fusion and exocytosis (600 s of observation time). However, spontaneous fusion events were rarely encountered in MIN6 cells (two spontaneous fusions in 12 observations; 2,375 s of observation, 304-μm^2 cell interfaces; 2.8×10^{-6} events per μm^2 per s). After depolarization, most docked GFP-granules remained fixed to the surface membrane. A limited number of vesicles fused at random time points after a median time of 50.3 s (75 events, 688-μm^2 cell interfaces, 1,515 s of observation, 7.2×10^{-5} events per μm^2 per second; or ≈26 times more common). In the example shown in Fig. 4 and Movie 3, which is published as supporting information on the PNAS web site, application of dextran–TMR 40 mM K^+ solution was followed by onset of two nearly simultaneous fusion events of syncollin–GFP vesicles (indicated by asterisks and small arrows). Note that each GFP-labeled granule filled with dextran–TMR (green + red = yellow; see also Movie 4, which is published as supporting information on the PNAS web site). Fusion of syncollin–GFP granules was also observed in isolated primary beta cells (Fig. 5*A*) as well as whole islets (data not shown). An example of exocytosis of PC3–GFP granules is shown in Fig. 5*B* (fusion of the vesicle occurs in *Center*).

In TIRF experiments, we used syncollin–GFP to serve as a content marker. All markers significantly colocalized with insulin, as judged by immunostaining with insulin in pancreatic beta cells and MIN6 cells. Both markers produced an increase in granule intensity at the moment of fusion similar to that described for pHluorins (26). The TIRF results show that the fusion events frequently led to complete release of protein (syncollin–GFP) combined with insulin in MIN6 cells. By TIRF, the incidence of full content release/fusion in MIN6 was 87% for GFP-syncollin (Fig. 6*A*, and Movie 5, which is published as supporting information on the PNAS web site), but only 33% for GFP-syncollin expressed in primary bovine chromaffin cells (gift from A. P. Fox, University of Chicago, Chicago) (Fig. 6*B*, and Movie 6, which is published as supporting information on the PNAS web site). The remaining events were incomplete, with granules remaining visible for extended periods. Those events might be classified as kiss and linger; "run" was very rarely observed in any system for GFP-labeled LDCVs (data not shown). In all cell types, syncollin–GFP rapidly diffused away, including chromaffin cells that lack granular proteases. Both optical methods report that the majority of insulin granules fully fuse with the cell membrane, and only rarely (a combined event rate of less than 15%) fail to fully collapse. TIRF microscopy offers superior time resolution, capturing fusion events at ≥30 images per s. However, the evanescence of the illumination creates uncertainty as to whether granules actually kiss and run or merely bob in the illumination, yet TIRF offers longer observation windows without photobleaching. Confocal microscopy is able to track granules deeper within cells and on surfaces of the cell other than the footprint.

Discussion

The coordination of regulated exocytosis of LDCVs in neuroendocrine cells is poorly understood. Numerous reports have detected partial vesicle fusions with rapid recovery or recycling commonly referred to as kiss-and-run fusions. In contrast to synaptic-vesicle-like fusions, our data support the classical "all or none" model (1–5, 23, 24) for insulin (LDCV) granule secretion. The comparison of data obtained by two imaging techniques,

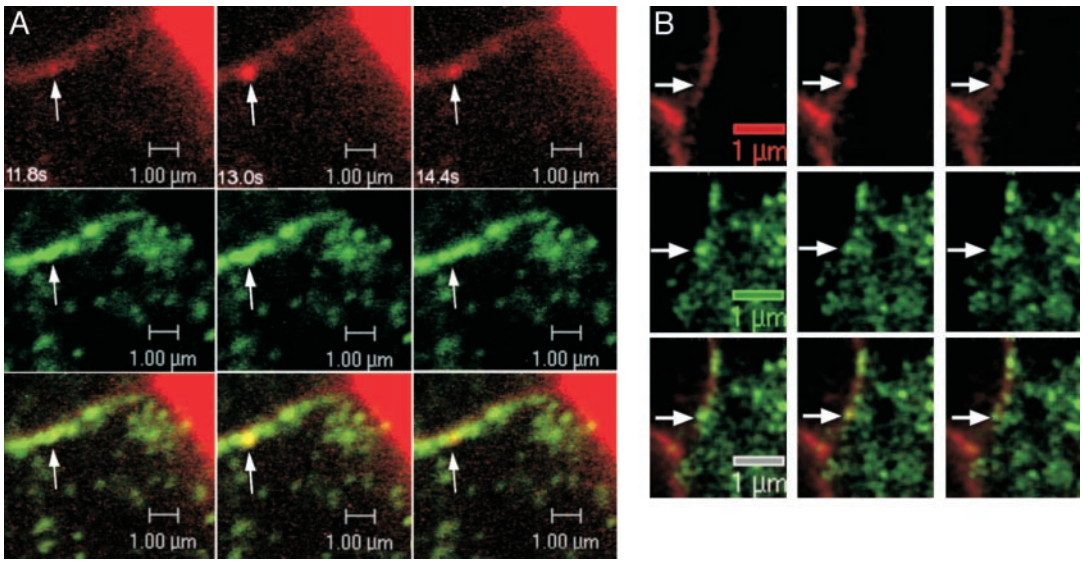

Fig. 5. Exocytosis of syncollin–GFP granules in isolated mouse beta cells and PC3–GFP granules in MIN6. (*A*) Exocytosis in isolated mouse beta cells. Interface between two cells (faint horizontal line) is filled with dextran–TMR (red) and shows development and collapse of omega-like figure in bottom cell. Syncollin–GFP is expressed only in lower cell. Colocalization of syncollin–GFP and dextran–TMR (*Lower*) results in yellow granule (arrows). Images were acquired 11.8, 13.0, and 14.4 s after depolarization. (*B*) Fusion (arrow) of a PC3–GFP granule in MIN6 cells; images were collected at 700 ms per scan (left to right). (Scale bars, 1 μm.)

TIRF and laser-scanning confocal microscopy with both granule and aqueous phase tracers, also strongly supports the concept that insulin granules are born in the Golgi. That is, insulin LDCV's are created *de novo*. Whether granule membrane recycling is a distinct event from general plasma membrane recycling is not clear. These conclusions are in general agreement with those for proteinaceous LDCV cargo in other cell types, such as acinar cells, and in clear distinction to the life cycle of synaptic granules (6–10, 15, 27). On the other hand, we found that LDCVs in bovine chromaffin cells labeled with the same probes showed both an all-or-none secretion and a kiss-and-run pattern, ensuring that our methods have the requisite sensitivity and temporal resolution to follow these events (Fig. 5).

Our results show that, during exocytosis, most insulin granules completely collapsed, as determined not only with large reporters such as syncollin–GFP (40 kDa) and PC3–GFP (90 kDa), but also with small molecule reporters (sulforhodamine B ≈500 Da and dextran–TMR ≈3 kDa; ≪ insulin ≈7 kDa). The full fusion of most insulin granules is consistent with the need to create protein-containing LDCV granules *de novo*. There was only rare evidence for rapid internalization of granule-sized vesicles from the plasma membrane in MIN6 cells. Other types of smaller secretory vesicles (e.g., γ-aminobutyric acid-containing) in beta cells could possibly use this distinct pathway (13, 28).

The combination of improvements in laser-scanning confocal TIRF microscopy and multicolor imaging enabled us to track the

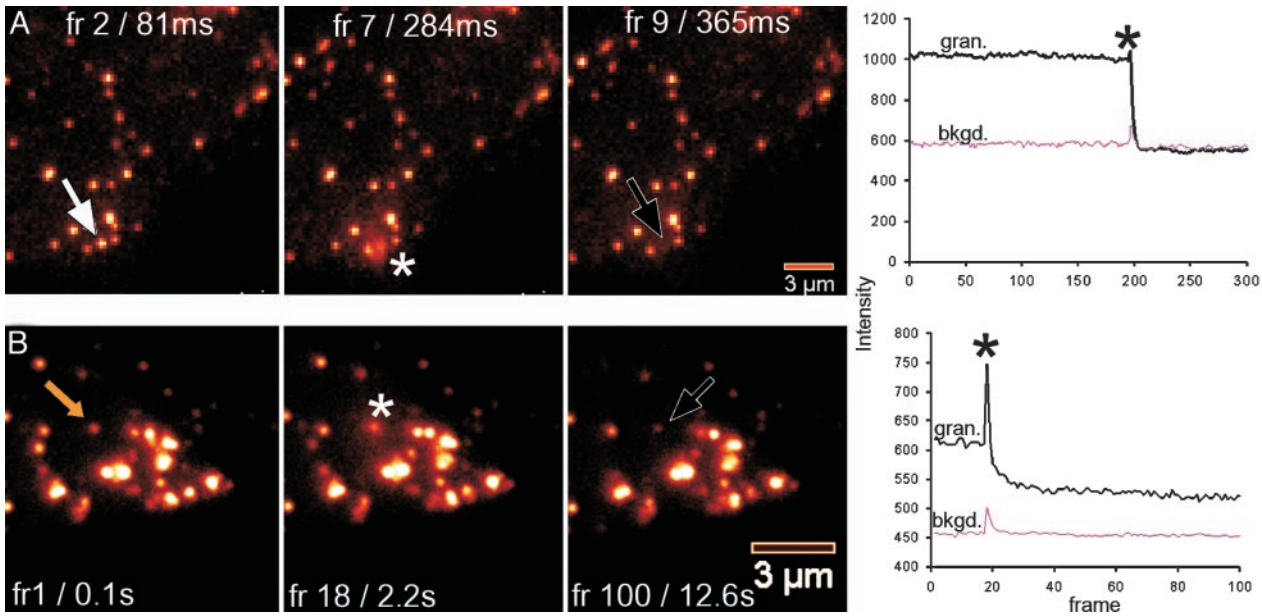

Fig. 6. TIRF images of syncollin–GFP -labeled granule exocytosis after depolarization with 40 mM KCl. (*A*) MIN6 cell (see Movie 5). (*B*) Primary bovine chromaffin cell (see Movie 6). Asterisks indicate the onset of granule fusions. (*Right*) Quantitation of intensity at the site of granule fusion (blue lines) and a nearby background (pink lines). Note the persistence of the granule after full disappearance in *A* and the partial discharge in *B*.

real-time destaining of single fluorescent-labeled insulin granules during exocytosis in beta cells and insulinoma cells. Although TIRF microscopy offers superior time resolution, the evanescence of the illumination creates uncertainty whether granules actually kiss and run or advance and retreat in the illumination. Confocal microscopy is able to track granules deeper within cells.

In summary, using two different GFP fusion proteins targeted to insulin granules in insulin secreting cells, we observed complete collapse of LDCVs to cell surfaces with only rare rapid-recycling/partial fusions. The predominance of full fusion of insulin granules was observed by using confocal as well as TIRF methodologies. In contrast, incomplete LDCV fusions were the rule in chromaffin cells. The predominance of complete fusion of insulin granules implies that endocytic retrieval of insulin granule membrane involves pathways other than direct refilling. Why insulin granules prefer full fusion and other LDCVs undergo partial/transient fusions remains unknown. Our live-cell imaging approaches may contribute to a new understanding of the mechanisms underlying exocytotic trafficking that can be ascertained directly and simultaneously in real-time.

We thank Ying Li Duan for preparing islets and Dr. Michael Roe for helpful discussion. We also thank the University of Chicago Integrated Microscopy Facility. This work has been partially supported by National Institutes of Health Grants DK44840, DK48494, DK63493, and DK20595 (Diabetes Research and Training Center at the University of Chicago) and the Blum–Kovler Foundation.

1. Kasai, H. (1999) *Trends Neurosci.* **22,** 88–93.
2. Barg, S. Eliasson, L., Renstrom, E. & Rorsman, P. (2002) *Diabetes* **51,** S74–82.
3. Bratanova-Tochkova, T. K., Cheng, H. Daniel, S., Gunawardana, S., Liu, Y. J., Mulvaney-Musa, J., Schermerhorn, T., Straub, S. G., Yajima, H. & Sharp, G. W. (2002) *Diabetes* **51,** S83–S90.
4. Dean, P. M. (1993) *Diabetologia* **9,** 115–119.
5. Lang, J. (1999) *Eur. J. Biochem.* **259,** 3–17.
6. Gundelfinger, E. D., Kessels, M. M. & Qualmann, B. (2003) *Nat. Rev. Mol. Cell. Biol.* **4,** 127–139.
7. Lang, T., Wacker, I., Steyer, J., Kaether, C., Wunderlich, I., Soldati, T., Gerdes, H. H. & Almers, W. (1997) *Neuron* **18**, 857–863.
8. Murthy, V. N. (1999) *Curr. Opin. Neurobiol.* **9,** 314–320.
9. Ohara-Imaizumi, M., Nakamichi, Y., Tanaka, T., Ishida, H. & Nagamatsu, S. (2002) *J. Biol. Chem.* **277,** 3805–3808.
10. Takahashi, N., Kishimoto, T., Nemoto, T., Kasowaki, T. & Kasai, H. (2002) *Science* **297,** 1349–1352.
11. Sankarayanan, S., De Angelis, D., Rothman, J. E. & Ryan, T. A. (2000) *Biophys. J.* **79,** 2199–2208.
12. Palfrey, H. C. & Artalejo, C. R. (2003) *Curr. Biol.* **13,** 397–399.
13. Braun, M., Wendt, A., Birnir, B., Broman, J., Eliasson, L., Galvanovskis, J., Gromada, J., Mulder, H. & Rorsman, P. (2004) *J. Gen. Physiol.* **123,** 191–204.
14. Tsuboi, T. & Rutter, G. A. (2003) *Curr. Biol.* **13,** 563–567.
15. Hodel, A. & Edwardson, J. M. (2000) *Biochem. J.* **350,** 637–643.
16. Ueda, K., Lipkind, G. M., Zhou, A., Zhu, X., Kuznetsov, A., Philipson, L. H., Gardner, P., Zhang, C. & Steiner, D. F. (2003) *Proc. Natl. Acad. Sci. USA* **100,** 5622–5627.
17. Ma, L., Tamarina, N., Wang, Y., Kuznetsov, A., Patel, N., Kending, C., Hering, B. J. & Philipson, L. H. (2000) *Diabetes* **49,** 1986–1991.
18. Miyazaki, J., Araki, K., Yamato, E., Ikegami, H., Asano, T., Shibasaki, Y., Oka, Y. & Yamamura, K. (1990) *Endocrinology* **127,** 126–132.
19. Tong-Chuan, H., Zhou, S., Da Costa, L. T., Yu, J., Kinzler, K. W. & Vogelstein, B. (1998) *Proc. Natl. Acad. Sci. USA* **95,** 2509–2514.
20. Ghadge, D. G., Lee, J. P., Bindokas, V. P., Jordan, J., Ma, L., Miller, R. J. & Roos, R. P. (1997) *J. Neurosci.* **17,** 8756–8766.
21. Clarendon, J. L., Phillips, C. L., Sandoval, R. M., Fang, S. & Dunn, K. W. (2002) *Am. J. Physiol.* **282,** C213–C218.
22. Waesle, B., Hays, L. B., Rhodes, C. J. & Edwardson, J. M. (2004) *Biochem. J.*, in press.
23. Orci, L., Amherdt, M., Malaisse-Lagae, F., Rouiller, C. & Renold, A. E. (1973) *Science* **179,** 82–84.
24. Orci, L., Perrelet, A. & Friend, D. S. (1977) *J. Cell Biol.* **75,** 23–30.
25. Somers, G., Blondel, B., Orci, L. & Malaisse, W. J. (1979) *Endocrinology* **104,** 255–264.
26. Miesenbock, G., De Angelis, D. A. & Rothman, J. E. (1998) *Nature* **394,** 192–195.
27. Holroyd, P., Lang, T., Wenzel, D., De Camilli, P. & Jahn, R. (2002) *Proc. Natl. Acad. Sci. USA* **99,** 16806–16811.
28. Nagamatsu, S., Nakamichi, Y., Watanabe, T., Matsushima, S., Yamaguchi, S., Ni, J., Itagaki, E. & Ishida, H. (2001) *J. Cell Sci.* **114,** 219–227.